Nanoscale

COMMUNICATION

View Article Online
View Journal | View Issue

Cite this: *Nanoscale*, 2014, **6**, 1271

Received 14th October 2013
Accepted 12th November 2013

DOI: 10.1039/c3nr05468c

www.rsc.org/nanoscale

Palladium nanosheets as highly stable and effective contrast agents for *in vivo* photoacoustic molecular imaging

Liming Nie,[ab] Mei Chen,[c] Xiaolian Sun,[a] Pengfei Rong,[a] Nanfeng Zheng*[c] and Xiaoyuan Chen*[a]

A stable and efficient contrast agent is highly desirable for photoacoustic (PA) imaging applications. Recently gold nanostructures have been widely reported and studied for PA imaging and photothermal therapy. However, the structures of the nonspherical gold nanoparticles are easily destroyed after laser irradiation and thus may fail to complete the intended tasks. In this study, we propose to apply palladium nanosheets (PNSs), with strong optical absorption in the near-infrared (NIR) region, as a new class of exogenous PA contrast agents. PA and ultrasound (US) images were acquired sequentially by a portable and fast photoacoustic tomography (PAT) system with a hand-held transducer. Significant and long-lasting imaging enhancement in SCC7 head and neck squamous cell carcinoma was successfully observed in mice by PAT over time after tail vein administration of PNSs. The morphology and functional perfusion of the tumors were delineated in PA images due to the nanoparticle accumulation. PAT of the main organs was also conducted *ex vivo* to trace the fate of PNSs, which was further validated by inductively coupled plasma atomic emission spectrometry (ICP-AES). No obvious toxic effect was observed by *in vitro* MTT assay and *ex vivo* histological examination 7 days after PNS administration. With the combination of a portable imaging instrument and signal specificity, PNSs might be applied as stable and effective agents for photoacoustic cancer detection, diagnosis and treatment guidance.

Introduction

At present, tissue biopsy is the most common way to accurately diagnose cancer. Having a noninvasive imaging method that could diagnose/image tumors would bring considerable benefit to patients by reducing unnecessary biopsies and surgeries. Photoacoustic tomography (PAT) with the aid of optimal exogenous contrast agents is very promising for diagnosis and visualization of superficial lesions such as the head and neck squamous cell carcinoma. Noninvasive and nonionizing PAT can potentially offer a painless diagnostic way to reduce the physical pain and emotional stress that a biopsy may cause.

PAT has been extensively studied in various biomedical applications to provide *in vivo* structural, functional, and molecular images.[1–3] The instrumentation of PAT has been implemented by several modalities, including photoacoustic microscopy,[4] full-ring ultrasonic array PAT,[5] and hemispherical array photoacoustic imaging.[6] The imaging specificity has always been an attractive research interest in PAT because function imaging is desired to monitor physiological dynamics with high contrast.

In order to enable the visualization of many other biomarkers besides hemoglobin and melanin, exogenous contrast agents were demonstrated to improve PAT imaging contrast and specificities.[7–11] Among these enhancing nanoparticles, gold nanostructures have been extensively reported and studied in PAT.[12–14] However, fabrication of a promising sensor candidate for optical monitoring still remains a great challenge since gold conjugates are very susceptible to heat/temperature rise. Stability of the administrated agents is an issue for continuous optical monitoring. Once melted, the particles will no longer be effective and will lose their functions for imaging or therapy purposes. For instance, gold nanorods begin to collapse dramatically after several minutes of laser irradiation with moderate energy.[12] Previously, palladium (Pd) nanosheets (PNSs) were reported to have high photothermal efficiency and catalytic properties.[15,16] Because of the high photothermal stability and ultrathin structure, PNSs hold great potential for imaging enhancement and cellular permeability in the biological system. However, to the best of our knowledge, the use of Pd for optical diagnostic imaging has never been reported.

In this study, we utilized a photoacoustic and ultrasound imaging system with a hand-held transducer for fast imaging

[a]*Laboratory of Molecular Imaging and Nanomedicine (LOMIN), National Institute of Biomedical Imaging and Bioengineering (NIBIB), National Institutes of Health (NIH), Bethesda, Maryland 20892, USA. E-mail: shawn.chen@nih.gov*

[b]*Center for Molecular Imaging and Translational Medicine, School of Public Health, Xiamen University, Xiamen 361005, China*

[c]*State Key Laboratory for Physical Chemistry of Solid Surfaces and Department of Chemistry, College of Chemistry and Chemical Engineering, Xiamen University, Xiamen 361005, China. E-mail: nfzheng@xmu.edu.cn*

acquisition, which is highly translatable into clinical medicine. For the first time, we applied PNSs as contrast agents with PAT for *in vivo* tumor perfusion visualization. The optical absorption and morphology changes of the PNSs *versus* gold nanostructures due to laser excitation were monitored by UV-vis-NIR spectroscopy and transmission electron microscopy (TEM), respectively. After 5 min laser irradiation at ~80 mW cm^{-2}, gold nanorods collapsed dramatically in structure and aggregated quickly. In contrast, the structure of PNSs remained almost unchanged even after 10 min laser irradiation. The tumor accumulation of the unique nanosheets is demonstrated on a head and neck squamous cell carcinoma (SCC7) xenograft model. Furthermore, the biodistribution of PNSs in different organs was measured *ex vivo* by PAT, which was validated by inductively coupled plasma atomic emission spectrometry (ICP-AES). *In vitro* MTT assay and *ex vivo* hematoxylin and eosin (H&E) staining were conducted to validate the nontoxicity of PNSs. Our study demonstrates that PNSs may be used as stable and effective agents for molecular photoacoustic imaging, which would greatly benefit early stage carcinoma evaluation, image-guided resection, and highly sensitive and specific staging.

Methods and materials

A high-resolution small-animal imaging system (Vevo LAZR 2100, VisualSonics, Canada) was employed for both ultrasound and photoacoustic imaging. A 256-element linear array transducer with a center frequency of 21 MHz was aligned to position the 10 mm focal depth in the center of the target. Ultrasound gel (Parker Laboratories, NJ), which does not produce any PA signal, was applied to the tissue surface for ultrasound signal coupling. Light from a tunable laser from 680–970 nm was delivered through an optical fiber bundle as the excitation source. A filtered back-projection algorithm was employed to reconstruct the PAT images.[17,18] The laser energy was recorded simultaneously to calibrate the laser energy fluctuation. Mice tumors were imaged using 790 nm laser light, before and after PNS probe injection. Ultrasound and PA images were obtained sequentially, and then overlapped into one image. The US image depicts the anatomy of the target while the PAT image reflects the functional optical absorption contrast.

To synthesize 16 nm palladium nanosheets, Pd(II) acetylacetonate ($Pd(acac)_2$, 10.0 mg), poly(vinylpyrrolidone) (PVP, MW ≈ 30 000, 30.0 mg) and NaBr (10.2 mg) were mixed together with *N*,*N*-dimethylvaleramide (2 mL) and water (4 mL) in a glass pressure vessel. The vessel was then charged with CO to 1 bar and heated at 60 °C for 3.0 h before it was cooled to room temperature. The mixture was kept at 4 °C overnight before centrifugation. The dark blue product was precipitated by acetone, separated by centrifugation and then purified using an ethanol–acetone mixture. The 16 nm hexagonal nanosheets exhibit absorption peaks at 790 nm.[19] The PNSs can be maintained in ethanol at 0 °C and still retain their NIR absorption characteristics even after several months. When used, the as-prepared dark blue solution was precipitated by acetone and separated *via* centrifugation at 10 000 rpm for 2 min. After centrifugation, the collected particles were dried by thorough lyophilization. Then the products were redispersed in water for imaging purposes. Photoacoustic and ultrasound imaging of tumors on two groups of mice were performed by injecting each with 200 μL of either PBS or 0.8 mg mL^{-1} PNS. All other chemicals were purchased from Sigma-Aldrich (St. Louis, MO, USA) unless stated otherwise.

Immunodeficient nude mice weighing ~21 g were used for the animal experiments. The SCC7 cells were cultured under standard conditions and inoculated subcutaneously into the shoulder of the mice (~10^6 cells per mouse). *In vivo* PAT and ultrasound imaging were performed 2 weeks after tumor growth with a diameter of ~0.9–1.3 cm. The mice were anesthetized with 1–2% isoflurane during experiments. The body temperature of the mice was maintained using a water heating system at 38 °C. After imaging, the mice were sacrificed and organs were harvested for biodistribution analysis of palladium by inductively coupled plasma atomic emission spectroscopy (ICP-AES). The ICP results were acquired from a JY2000 Ultrace ICP atomic emission spectrometer equipped with a JY AS 421 autosampler and 2400 g mm^{-1} holographic grating. Samples ($n = 5$ per tissue) for ICP-AES analysis were lyophilized, and dissolved in *aqua regia* under minor stirring for 12 h until the palladium particles were fully dissolved.[20] The *aqua regia* was prepared with 100 μL of nitric acid and 300 μL of 37% hydrochloric acid. Then the samples were diluted to 10 mL with 9.6 mL of 2% HNO_3 and analyzed *via* ICP-AES.

The *in vitro* cytotoxicity of PNSs was analyzed using a standard methyl thiazolyl tetrazolium (MTT, Sigma-Aldrich) assay. SCC7 cells were seeded into a 96-well plate at a density of 10^4 cells per well and then incubated at 37 °C for 24 h under 5% CO_2. After incubating SCC7 cells with PNSs at various concentrations for 24 h, the standard MTT assay was carried out to determine the cell viability relative to the control untreated cells. For H&E staining, mice injected with either PBS (control) or PNSs (20 mg kg^{-1}) were sacrificed at 7 days post-injection. Major organs were harvested and sectioned into thin slices for histological analysis. All animal procedures were approved by the Institutional Animal Care and Use Committee of the Clinical Center, National Institutes of Health.

Results and discussion

The photothermal properties of gold nanorods (GNRs) and PNSs after various periods of laser irradiation were investigated by UV-vis-NIR spectra measurement. The tested GNRs were well dispersed in water with an aspect ratio of 3 : 1. The UV-vis-NIR spectra of GNRs were acquired before, 5, 10, and 15 min after laser irradiation (Fig. 1a). The laser energy was ~4 mJ per cm^2 per pulse with a repetition rate of 20 Hz, which is the energy source for PAT. After 5 min laser irradiation, the spectrum curve changed to a plateau and the relative absorption peak dropped sharply from nearly 1.0 to less than 0.2. Over the next 10 min of irradiation there was further smoothing to the absorption curve. There was also a shift in peak absorption towards shorter wavelengths within the first 5 min, from 850 nm to ~740 nm. In contrast, the absorption spectra of PNSs remained almost

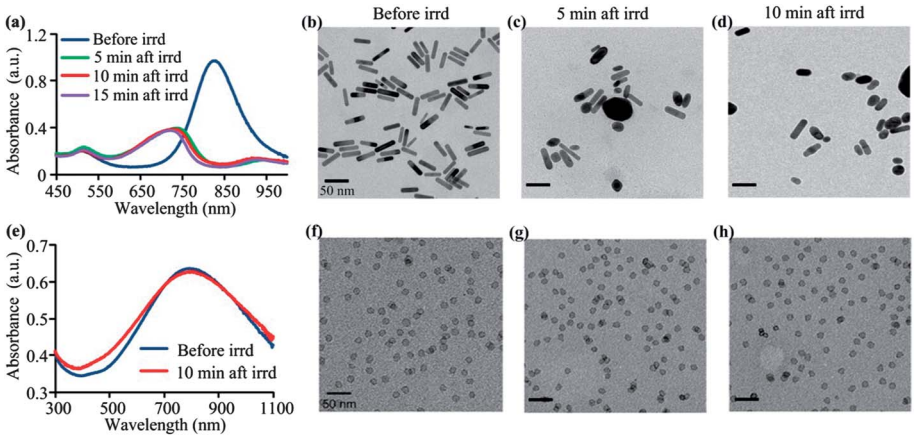

Fig. 1 (a) Absorption spectra of gold nanorods (GNRs, 3 : 1 aspect ratio) before, 5, 10, and 15 min after laser irradiation. (b–d) TEM images of the GNRs (b) before, (c) 5 min, and (d) 10 min after pulsed laser irradiation. (e) Absorption spectra of palladium nanosheets (PNSs) before and 10 min after laser irradiation. (f–h) TEM images of the PNSs (f) before, (g) 5 min, and (h) 10 min after pulsed laser irradiation. The pulsed laser was set at ~4 mJ per cm^2 per pulse with a repetition rate of 20 Hz.

unchanged with slight broadening 10 min after laser irradiation (Fig. 1e). Specifically, the relative optical extinction fluctuated by less than 0.1% after 10 min of irradiation, as compared to the initial value.

Correspondingly, TEM images of GNRs before, 5 min, and 10 min after laser irradiation are displayed in Fig. 1b–d, respectively. It is interesting to observe that during the irradiation period, a shorter and rounder structure takes the place of the distinct long and rod shape of the GNS. Moreover, the gold nanoparticles aggregated and accreted severely to exhibit dark 'spots' in the TEM images. Since the plasmonic resonance is determined by the molecular conformation, the optical absorbance differences depicted in Fig. 1a can be explained by the morphological change caused by laser irradiation. However, in comparison, there was hardly any change in the PNS shape during the irradiation period, as shown in the TEM images of Fig. 1f–h. Compared to GNRs, PNSs are much more stable at maintaining both their morphology and peak absorption throughout the laser irradiation. The results in Fig. 1 demonstrate that the as-prepared palladium compound is ideally stable under long-term laser irradiation.

The dynamic light scattering (DLS) method was also employed to further validate the phothermal stability of PNSs (Fig. 2a). The hydrodynamic size of PNSs after 10 min laser irradiation with a pulse energy of 4 mJ cm^{-2} was very similar to that before laser irradiation, corroborating with the UV-vis-NIR and TEM results. The PA signal as a function of nanoparticle concentration is shown in Fig. 2b. PNS solutions were filled in transparent thin tubes. Note that both the top and bottom boundaries of the tubes were clearly delineated in the PAT images because the 21 MHz ultrasonic transducer filtered out the low-frequency components from the center of the tubes. A strong linear relationship ($n = 4$ per group, $R^2 = 0.995$) was found between the produced PA signal intensity and the concentration of PNSs.

PAT and ultrasound images of two groups of mice ($n = 5$ per group) bearing SCC7 xenografts were acquired at 2, 4, 6, 8, and 24 h after tail vein injection of either PBS (200 μL) or PNSs (200 μL, 0.8 mg kg^{-1}) (Fig. 3). The PAT image displayed in color and the ultrasound image displayed in gray were overlayed for each time point. The 790 nm laser with moderate laser energy at ~4 mJ cm^{-2} was used for PA probe detection. As shown in Fig. 3a, only tumor skin produced PA signals on the surface of the mice injected with PBS, which is attributable to the shallow penetration depth and low absorption contrast in the tumor.

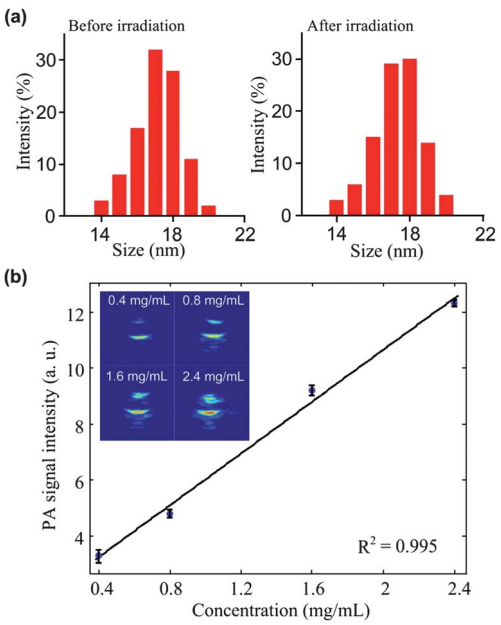

Fig. 2 (a) Size distribution of palladium nanosheets (PNSs) measured by dynamic light scattering (DLS) before and 10 min after pulsed laser irradiation (4 mJ per cm^2 per pulse with a repetition rate of 20 Hz). (b) Linear regression plot of the relative PA signal intensity and PNS concentration. The error bars represent standard error ($n = 4$ per group). The original PA image for each concentration was also displayed in the upper left corner.

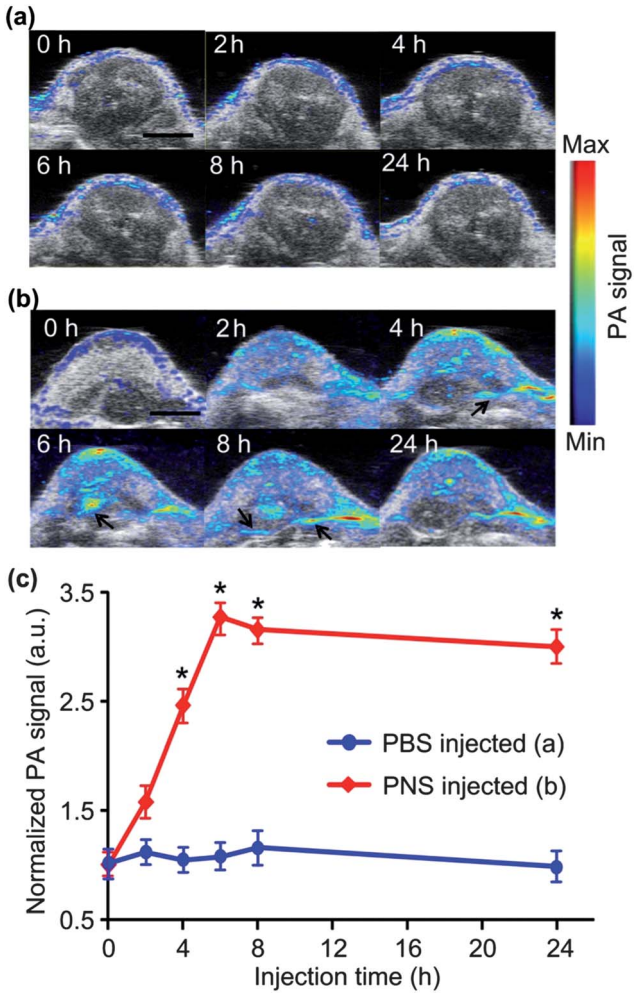

Fig. 3 Photoacoustic and ultrasound images of tumors on two mice groups injected intravenously with 200 μL of (a) PBS and (b) 0.8 mg mL^{-1} PNS solutions acquired at 0, 2, 4, 6, 8, and 24 h post-injection, respectively. The arrows show more features in the tumor enhanced by the Pd agents. Scale bar = 5 mm. (c) Quantified PA signal in the tumors injected with PBS and PNSs acquired before, 2, 4, 6, 8, and 24 h after injection. The PA signals in each group were self-normalized for comparison between two groups. The error bars represent standard error (n = 5 per group, P < 0.01).

However, the image contrast of the tumor in Fig. 3b injected with PNSs gradually increased, indicating that a significant amount of PNSs were gradually accumulating into the tumor to enhance the visibility. The ultrahigh tumor accumulation of PNSs is likely due to the enhanced permeability and retention (EPR) effect in cancerous tumors with tortuous and leaky vasculatures. Most importantly, with the aid of PNSs, the lower boundary of the tumor was unveiled in the images, which could be potentially used for guiding surgery.

In each image, PA signals were selected and quantified within an identical region of interest (ROI) with a diameter of 1 cm. The average value of the calculated PA signals was shown to evaluate the variation of nanoparticle accumulation in the tumor area (Fig. 3c). The PA signals in each group were self-normalized for comparison between two groups. Specifically, the PA signals at different time points were divided by the PA signal before injection. The red line represents the group injected with PNSs while the blue line represents the group injected with pure PBS. For the PNS group, the PA signal achieved in the tumor is 3.5-fold greater than the original signal and reached a steady level even after 24 h. Statistical significance between the two groups was assessed at each time point using a two-tailed Student's t-test. It indicates that PNSs produced a more persistent and efficient PAT enhancement (*, P < 0.01). The results suggest that the molecular specific PAT with plasmonic Pd nanocrystals could be used to enhance the embedded tumor and uncover the boundaries.

To trace the fate of PNSs in the mice, *ex vivo* PAT at 790 nm was carried out on the main organs of the two mice groups (n = 5 per group) before and 24 h after PNS injection (200 μL, 0.8 mg mL^{-1}). The photos of the organs (liver, spleen, heart, lung, and kidney) are shown in Fig. 4a. PAT images of the organs from the mice before and 1 day after injection with PNSs are shown in Fig. 4b and c, respectively. As can been seen, the liver has more palladium deposition, which is about 4 times higher than that in the spleen and lung. The results of this *ex vivo* study may fluctuate due to surgical procedures, laser wavelength, blood distribution in the organs, *etc.* However, the method could be useful for quick measurement in animal studies especially when the direct measurement is not possible.

Furthermore, the biodistribution of Pd in the organs 24 h after injection was measured by ICP-AES. The statistical results with standard deviations are shown in Fig. 5a. The liver has the highest accumulation, which is consistent with the PA measurement result. The tumor contained the second highest palladium concentration, which was also observed with the positive PA signal amplification in the tumor. The other organs, such as the kidneys, heart, spleen, and lung, also had some accumulation of Pd. The nanoparticle accumulation variations on the organs depend on the particle properties (size, surface modification, shape, structure, charge, *etc.*) and experimental design (animal model, dosage, method and time schedule of administration, observation time, *etc.*).[21,22] Therefore, further careful and comprehensive studies of nanobiosafety are needed to determine the biodistribution–accumulation–retention–clearance effects of PNSs and their roles in toxicity.

As illustrated in Fig. 5b, the viabilities of cells exposed to various concentrations of PNSs show a similar pattern to that of the control cells, indicating that PNSs below the concentration of 1 mg mL^{-1} are essentially non-toxic to SCC7 cells. Since the Pd nanoparticles were entrapped in the liver and spleen indicated by ICP-AES, macrophages in the liver (Kupffer cells) and spleen were assumed to have absorbed the majority of the nanoparticles. However, the histological image of the hepatic lobules did not display an elevated number of Kupffer cells 7 days after PNS injection compared to PBS control (Fig. 5c). Macrophages in the marginal area of the spleen did not show any apparent change, either. Mesangial cell proliferation with expansion is usually observed in

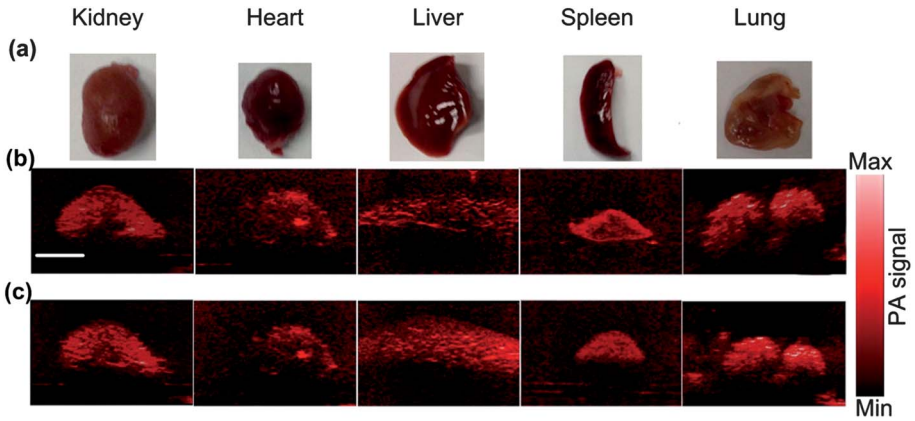

Fig. 4 *Ex vivo* PAT of the main organs before and 24 h after tail vein injection of PNSs (200 μL, 0.8 mg mL^{-1}). (a) Photograph of the organs (kidney, heart, liver, spleen, and lung). (b) PAT images of the organs from the mice before injection of PNSs. (c) PAT images of the organs from the mice 1 day after injection of PNSs. Scale bar = 2 cm.

glomerulonephritis. However, we did not observe obvious change in the number of positively stained mesangial cells in the kidneys of mice injected with PNSs compared with PBS control. No noticeable abnormality was observed in major organs including kidneys, heart, liver, spleen, lung, stomach and intestine. Although our preliminary data here showed that PNSs could offer good biocompatibility, future experiments are still needed to interpret the long-term fate, clearance pathways, and toxicology of PNSs in animals.

Owing to the significantly higher bulk melting point (MP_{Pd} = 1828 K *versus* MP_{Au} = 1337 K, and MP_{Ag} = 1235 K), PNSs, in principle, should possess improved photothermal stability over gold and silver nanostructures. Furthermore, the unique nanosheets have a large surface area because of their ultrathin character (<10 atomic layers thick),[15,23] which could be used for high-loading drug delivery. Although PNSs may be possibly excreted *via* both fecal and renal clearance, better understanding of long-term toxicology and quantitative pharmacokinetics is important and requires further investigations. Previous studies indicate that nanoparticles with a size of dozens of nanometers may exhibit higher tumor accumulation ability than bigger nanoparticles due to their minimal recognition by the liver and spleen macrophages,[24,25] which encouraged us to apply 16 nm PNSs in this study. More systematic investigations on PNSs with larger sizes are currently underway.

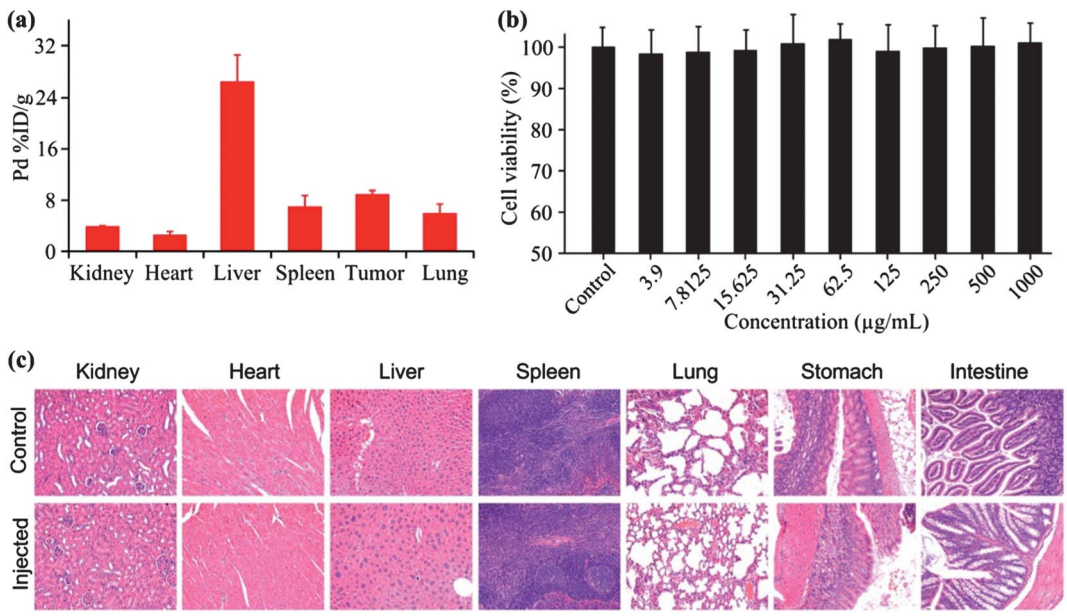

Fig. 5 (a) Biodistribution of Pd in main organs (kidneys, heart, liver, spleen, tumors and lung) of the mice at 24 h post-injection of PNSs (200 μL, 0.8 mg mL^{-1}) acquired by ICP-AES. (b) SCC-7 cell viability after 48 h exposure to PNSs at different concentrations. (c) H&E staining of various major organs of nude mice 7 days after administration of PBS (control) or PNSs (20 mg kg^{-1}). No noticeable abnormality was observed in major organs including kidneys, heart, liver, spleen, lung, stomach, and small intestine.

Conclusions

In summary, we demonstrated the feasibility of palladium nanosheets (PNSs) as a novel class of probes for *in vivo* tumor perfusion imaging. The tumor morphology and boundaries were greatly enhanced in the PAT images, suggesting that PNSs can produce a stable and effective means for optical tumor labeling and visualization. Currently only 4 mJ per cm^2 per pulse energy is used, which is well below 20 mJ per cm^2, the safety standard set by the American National Standards Institute (ANSI).[26] Therefore, with relatively strong laser energy for deeper tissue penetration, quantitative measurement of nanoparticle accumulation *in vivo* by PAT will be possible in the future. Moreover, our PA/US system is highly mobile and does not require complicated alignment. It takes only 0.05 second (20 Hz) to acquire one PAT image with a real-time ultrasound image, which is fast enough to catch the most physiological changes in the tumor.

Since the tumor has the second highest PNS accumulation next to the liver in our study, the imaging strategy may also be used for *ex vivo* differentiation and characterization of malignant tumors. We believe that the proposed PNS formula and imaging method are very promising for photoacoustic imaging of tumors.

Acknowledgements

This project is supported in part by the National Science Foundation of China (81301257, 81371596), the National Basic Research Program of China (973 program 2013CB733802, 2014CB744503), and by the intramural research program of the National Institute of Biomedical Imaging and Bioengineering. We also thank summer intern Mr. Eshwar Manoharan for the editorial assistance.

References

1 D. Razansky, C. Vinegoni and V. Ntziachristos, *Opt. Lett.*, 2007, **32**, 2891–2893.
2 B. Cox, J. G. Laufer, S. R. Arridge and P. C. Beard, *J. Biomed. Opt.*, 2012, **17**, 061202.
3 L. M. Nie, D. Xing and S. H. Yang, *Med. Phys.*, 2009, **36**, 3429–3437.
4 Y. Zhang, X. Cai, S. W. Choi, C. Kim, L. V. Wang and Y. Xia, *Biomaterials*, 2010, **31**, 8651–8658.
5 J. Xia, M. R. Chatni, K. Maslov, Z. J. Guo, K. Wang, M. Anastasio and L. V. Wang, *J. Biomed. Opt.*, 2012, **17**, 050506.
6 D. Van de Sompel, L. S. Sasportas, A. Dragulescu-Andrasi, S. Bohndiek and S. S. Gambhir, *PLoS One*, 2012, **7**, e45337.
7 L. Nie, S. Wang, X. Wang, P. Rong, Y. Ma, G. Liu, P. Huang, G. Lu and X. Chen, *Small*, 2013, DOI: 10.1002/smll.201302924.
8 X. Cai, W. Li, C. H. Kim, Y. Yuan, L. V. Wang and Y. Xia, *ACS Nano*, 2011, **5**, 9658–9667.
9 L. Nie, Z. Ou, S. Yang and D. Xing, *Med. Phys.*, 2010, **37**, 4193–4200.
10 A. A. Bhirde, G. Liu, A. Jin, R. Iglesias-Bartolome, A. A. Sousa, R. D. Leapman, J. S. Gutkind, S. Lee and X. Chen, *Theranostics*, 2011, **1**, 310–321.
11 Z. Chen, L. Ma, Y. Liu and C. Chen, *Theranostics*, 2012, **2**, 238–250.
12 M. S. Yavuz, Y. Cheng, J. Chen, C. M. Cobley, Q. Zhang, M. Rycenga, J. Xie, C. Kim, K. H. Song, A. G. Schwartz, L. V. Wang and Y. Xia, *Nat. Mater.*, 2009, **8**, 935–939.
13 S. Mallidi, T. Larson, J. Tam, P. P. Joshi, A. Karpiouk, K. Sokolov and S. Emelianov, *Nano Lett.*, 2009, **9**, 2825–2831.
14 E. Y. Lukianova-Hleb, X. Ren, D. Townley, X. Wu, M. E. Kupferman and D. O. Lapotko, *Theranostics*, 2012, **2**, 976–987.
15 X. Huang, S. Tang, X. Mu, Y. Dai, G. Chen, Z. Zhou, F. Ruan, Z. Yang and N. Zheng, *Nat. Nanotechnol.*, 2011, **6**, 28–32.
16 L. Vu, J. Ramos, T. Potta and K. Rege, *Theranostics*, 2012, **2**, 1160–1173.
17 L. Nie, D. Xing, Q. Zhou, D. Yang and H. Guo, *Med. Phys.*, 2008, **35**, 4026–4032.
18 B. T. Cox, J. G. Laufer and P. C. Beard, *Biomed. Opt. Express*, 2010, **1**, 201–208.
19 H. Li, G. Chen, H. Yang, X. Wang, J. Liang, P. Liu, M. Chen and N. Zheng, *Angew. Chem., Int. Ed.*, 2013, **52**, 8368–8372.
20 A. Lopez-Molinero, O. Mendoza, A. Callizo, P. Chamorro and J. R. Castillo, *Analyst*, 2002, **127**, 1386–1391.
21 W. T. Al-Jamal, K. T. Al-Jamal, B. Tian, A. Cakebread, J. M. Halket and K. Kostarelos, *Mol. Pharm.*, 2009, **6**, 520–530.
22 P. Decuzzi, B. Godin, T. Tanaka, S. Y. Lee, C. Chiappini, X. Liu and M. Ferrari, *J. Controlled Release*, 2010, **141**, 320–327.
23 M. Chen, B. Wu, J. Yang and N. Zheng, *Adv. Mater.*, 2012, **24**, 862–879.
24 W. H. De Jong, W. I. Hagens, P. Krystek, M. C. Burger, A. J. A. M. Sips and R. E. Geertsma, *Biomaterials*, 2008, **29**, 1912–1919.
25 S. M. Moghimi, A. C. Hunter and J. C. Murray, *Pharmacol. Rev.*, 2001, **53**, 283–318.
26 L. I. o. America, *ANSI Z136.1*, American National Standards Institute, New York, 2000.

